Near-Source Seismic Demand and Pulse-Like Records: a Discussion for L'Aquila Earthquake.

Eugenio Chioccarelli and Iunio Iervolino[◊]

Dipartimento di Ingegneria Strutturale, Università degli Studi di Napoli Federico II,
Via Claudio 21, 80125, Naples, Italy.

SUMMARY

Rupture directivity effects in ground motion are known since many years to both seismologists and earthquake engineers; i.e., in sites that are in a particular geometrical configuration with respect to the rupture, the velocity fault-normal signals may show a large pulse which occurs at the beginning of the record and contains the most of energy. The results are waveforms different from ordinary ground motions recorded in the far field or in geometrical conditions not favorable with respect to directivity. Current attenuations laws are not able to capture such effect well, if at all, and current probabilistic seismic hazard analysis is not able to predict the resulting peculiar spectral shape. Moreover, it is believed that structures with dynamic behavior in a range of periods related to the pulse period may be subjected to underestimated seismic demand. In the paper this is investigated and increments in both elastic and inelastic seismic actions are quantified using a large dataset of records, from the next generation attenuation project (NGA), in which a fraction is comprised of velocity pulses identified in other studies. These analyses employ recently developed tools and procedures to assess directivity effects and to quantify the associated threat in terms of seismic action on structures. Subsequently, the same tools are used in one of the first attempts to identify near-source effects in the data recorded during a normal faulting earthquake, the mainshock of the recent Abruzzo (central Italy) sequence, leading to conclude that pulse-like effects are likely to have occurred in the event, that is: (1) occurrence of pulse-like records in some near-source stations is in fair agreement with existing predictive models; (2) the increment in seismic demand shown by pulse-like ground motion components complies with the results of the analysis of the NGA data; (3) seismic demand in non-impulsive recordings is generally similar to what expected for ordinary records. The results may be useful as a benchmark for inclusion of near-source effect in design values of seismic action and structural risk analysis.

Keywords: ground motion, seismic hazard, seismic action, near-source, directivity.

1 INTRODUCTION

In the case of an earthquake, ground motion recorded at near-source sites may be subjected to rupture directivity effects which result in a low frequency full cycle velocity pulse at the beginning of the signal. The occurrence of this effect depends on the rupture process and on the geometrical configuration of the fault and the site. More specifically, according to Somerville et al. [1], the seismic energy radiated from the source arrives almost in single large pulse of motion if: the rupture propagates toward the site, the direction of slip on the fault is aligned with the site, and the propagation velocity of rupture is almost as large as the shear wave velocity. Figure 1a sketches rupture directivity effect in the simple case of an unilateral strike-slip fault. As the rupture, which may be seen as a point source moving along the fault, goes away from the epicenter, it radiates energy in seismic waves originated at different instants. Roughly speaking, the wave fronts tend to all arrive at the same time in site 2, this may be seen as *constructive interference* of waves. Conversely, in site 1, with respect to

---
[◊] Corresponding author. Address: Dipartimento di Ingegneria Strutturale, Università degli Studi di Napoli Federico II, via Claudio 21, 80125, Naples, Italy. Tel: +390817683488; Fax: +390817683491; iunio.iervolino@unina.it.

which the rupture moves away, waves radiated in different instants tend also to arrive in different moments. Therefore, in the former case the energy is concentrated in a high amplitude and short duration (impulsive) motion, while in the latter the energy is spread over a larger amount of time and in an lower amplitude signal [2,3].

Because of the radiation pattern, in the case of strike-slip ruptures, directivity pulses are oriented in the strike-normal direction that corresponds to the fault-normal direction [1]. In dip-slip earthquakes, the rupture directivity pulse is expected in the direction normal to the fault dip, and should have components in both the vertical and the horizontal strike-normal direction [1] [4]. In the strike-parallel direction minor directivity effects, if any, are expected. Hereinafter, horizontal ground-motion components in strike-normal and strike-parallel directions will be referred to as fault-normal (FN) and fault-parallel (FP), Figure 1b.
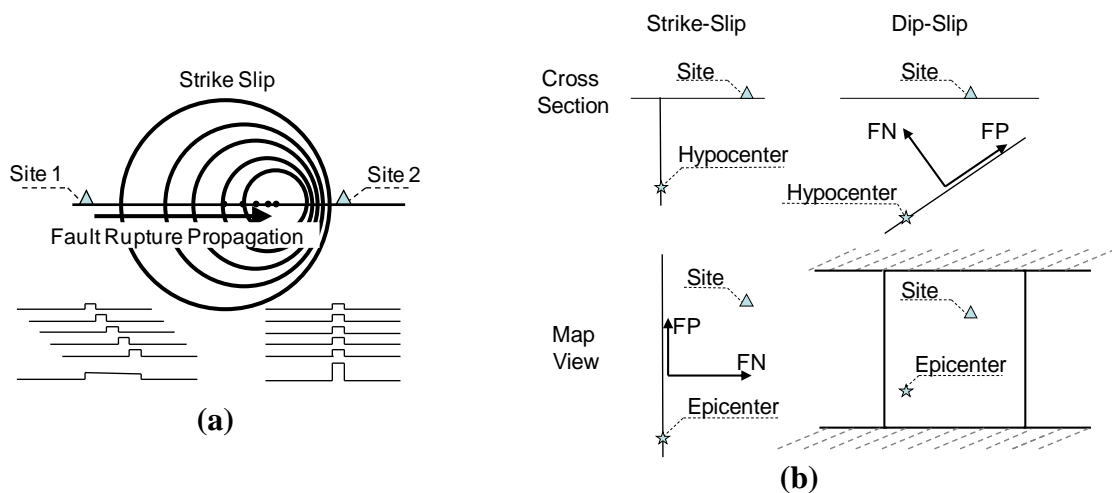
Figure 1. (a) Directivity of seismic energy: snapshot of wave fronts (adapted from Singh [2]); (b) directions of effects' observation for strike-slip and dip-slip cases (adapted from Somerville [4]).

Because rupture and propagation of waves in actual earthquakes are much more complex than what just discussed, other factors perturb the conditions to clearly observe velocity pulses and not all near-fault locations experience forward directivity effects in a given event; conversely, directivity may occur at sites apparently not prone to pulse-like ground motion [5]. On the other hand, pulse-type records are of interest to structural engineering because the seismic action is expected to be peculiar with respect to non-pulse-like records (*ordinary* in the following), that is: (1) the elastic demand of pulse-like signals is generally larger than that of ordinary recordings, particularly concerning the fault-normal direction; (2) the spectral shape is non-standard with an increment of spectral ordinates in the range around the pulse period; (3) because the pulse period is generally a low frequency one (i.e., in the same order of magnitude of that of the most of common structures) the inelastic demand can be particularly high [6] and developed in a comparatively short time which may facilitate fragile collapse mechanisms in structures not properly designed. Finally, although this paper focuses on low frequency pulse-like records, it is to recall that some researchers (e.g., [7]) also believe directivity may affect peak values of motion as peak ground acceleration (PGA).

---

[1] It is to recall that in dip-slip earthquake also the *fling step* may appear in the strike-normal direction. It is related to the permanent ground deformation (i.e., residual displacement) and results in a half cycle pulse, differing from directivity which is expected to be a full cycle pulse [1].

In the following the amplification of elastic and inelastic seismic demands for pulse-like fault-normal records and the peculiar spectral shape driven by the pulses are investigated first with respect to fault-parallel and non-pulse-like near-source motions. The dataset is a subset of FN- and FP-rotated records from the next generation attenuation project (NGA) database and analyzed by Baker [8]. The results from this analysis may help the current research undergoing to adjust probabilistic seismic hazard analysis to account for pulse-like records occurrence [9] and to quantify the structural effects [6,10]. Herein they are also used as a benchmark to investigate directivity effects in the recent April 6th 2009 L'Aquila earthquake (moment magnitude or, M_w, 6.3). In particular, near-source records from the mainshock, rotated in FN and FP directions, were analyzed to extract pulses with the same procedure used for the NGA dataset. Those found as likely containing velocity pulses were compared to: (1) those not identified as pulse-like; (2) the un-rotated components, and (3) to predictive models for the occurrence of directivity pulses and for the pulse period. The features of L'Aquila records were also compared to those of the NGA database to check whether they are in agreement to what expected for impulsive and non impulsive near-source records. The analyses include also rupture-rotated and vertical components of motion.

2   PULSE-LIKE SEISMIC ACTION

In order to identify the peculiar features of impulsive signals in terms of seismic action on structures, a dataset from the NGA database (http://peer.berkeley.edu/products/nga_project.html) was considered. It determinedly includes records identified as pulses as well as signals in which the pulses were not found, this is required to enlighten the specific characteristics, in terms of structural demand, of pulse-like records. NGA records, in fact, were classified as "pulse-like" and "non-pulse-like" by Baker [8] via a wavelets-based algorithm, which assigns a score, a real number between 0 and 1, to each record and determines the pulse period (Tp). The larger the score the more likely the record is to show a pulse. Only the fault-normal ground motions having a pulse score equal or larger than 0.85 were, arbitrarily, counted as pulse-type records. Note that pulses may possibly be indentified also in fault-parallel components, but these cases are not counted herein within the group of pulse-like records, although the behavior of FP components is investigated for those ground motions where FN is pulse; moreover, the algorithm does not detect fling as the wavelet functions used have zero residual displacement. In fact, the considered pulse-like signals are the same utilized in [9]: this selection slightly differs from that proposed by Baker [8] but it is based on the analysis of the same database. It consists of 73 records from 23 events, 12 of which are strike-slip (Table 1).

Table 1. Analyzed NGA records.

Type	Events	Records	Pulse-Like Records
Strike-Slip	12	133	34
Non-Strike-Slip	11	229	39
Total	*23*	*352*	*73*

The events' M_w ranges from 5.2 to 7.5. The number of records from strike-slip events is 133, the records identified as pulses in the given dataset are 34. Other records coming from other faulting mechanisms which are non-strike-slip are 229, 39 of which are identified as pulses (see [9] for details and for a complete list of pulse-like records). Note that in the following no distinction will be applied to records from different faulting styles, as results of the analyses do not support to keep such a difference.

2.1 Elastic demand and spectral shape

The first peculiarity of pulse-like records is related to the elastic seismic demand. To investigate it, the ratio of elastic spectral displacement at various periods (T) in the FN direction, $S_{d,e\ FN}(T)$, with respect to the FP component, $S_{d,e\ FP}(T)$, was computed. It is expected that because the pulse is to be observed mostly in the fault-normal component, the FN over FP ratio is larger for ground motions where the FN is identified as pulse-like with respect to records where FN is non-pulse-like. This is given in terms of average of the natural logarithm, as a function of the T over Tp ratio, in Figure 2a. Dashed lines are the averages plus and minus one standard deviation. Although dispersion is very high, as usually happens for ground motion amplitudes, it is quite clear that, if there are pulse-like signals, elastic FN demand is about 50% higher than FP (maximum value of FN over FP spectral displacement ratio is 1.57). Conversely, if there are no pulse-like signals in the fault-normal component, seismic demands in FN and FP directions are comparable. The second feature investigated, and probably the most important, is the peculiar spectral shape of pulse-like signals. In fact, spectra of these records have an increment of acceleration ordinates (or a "bump") in a range of periods around Tp. This is particularly critical as current attenuation relationships are not able to describe it and therefore seismic hazard and demand analyses may be potentially un-conservative. In Table 2 the pulse periods found in the dataset are divided in bins and for each bin the number of pulse-like records is shown. In Figure 2b the average elastic acceleration spectra of pulse-like records for some of the bins, the most significant for the dynamic behavior of ordinary structures, are given. To compare different ground motions, all spectra were normalized; i.e., all ordinates (Sa) were divided by the PGA. It may be observed the non-standard shape of pulse-like records.

Table 2. Number of records for bins of Tp.

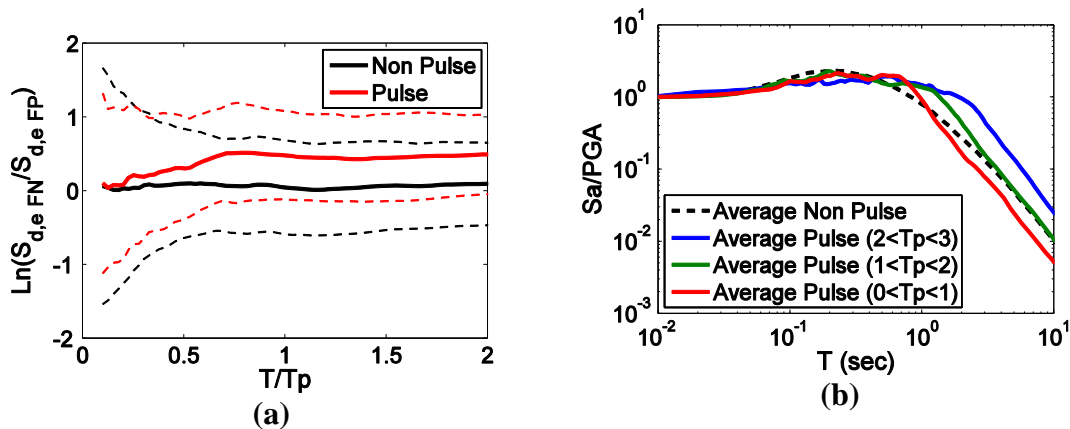| Tp	[0s,1s[	[1s,2s[	[2s,3s[	[3s,4s[	[4s,5s[	[5s,6s[	[6s,12s[
No. of records	18	18	8	10	9	5	5

(a)   (b)

Figure 2. (a) FN/FP elastic displacement ratios; (b) Average elastic acceleration spectra for bins of Tp.

However, normalization by means of PGA, used in Figure 2b, works in the high frequency range only. Therefore, the elastic demand should be better analyzed considering the deviations of the considered ground motion intensity measure (IM) from what computed by an appropriate ground motion prediction equation (GMPE or *attenuation law*); i.e., the ε values in Equation 1.

$$\varepsilon = \Big[\log(IM) - \overline{\log(IM)} \Big] \Big/ \sigma_{\log(IM)} \tag{1}$$

In Equation 1: IM is the recorded ground motion parameter; $\overline{\log(IM)}$ is the mean of the logarithms of IM obtained from the attenuation relationship; and $\sigma_{\log(IM)}$ is the standard deviation of the logarithms of IM, still from the GMPE. The used GMPE is that from Boore and Atkinson [11] and Figure 3 shows the ε values [2], for the FN and FP components in the case of pulse-like (a) and non-pulse-like (b) ground motions. Results of ε for pulse-like records before rotation have a bump around T equal to Tp, but it is never higher than 1. FN-rotated records have the same shape but they have maxima close to 2. In the case of ground motions where FN is identified as non-pulse-like, ε does not show a clear trend [3] (Figure 3b). Moreover, rotation does not affect the results significantly. Comparison of pulse-like and non-pulse-like records also shows that ε values in the former case are systematically higher than the latter confirming that the pulse-like are generally stronger than non-pulse-like.
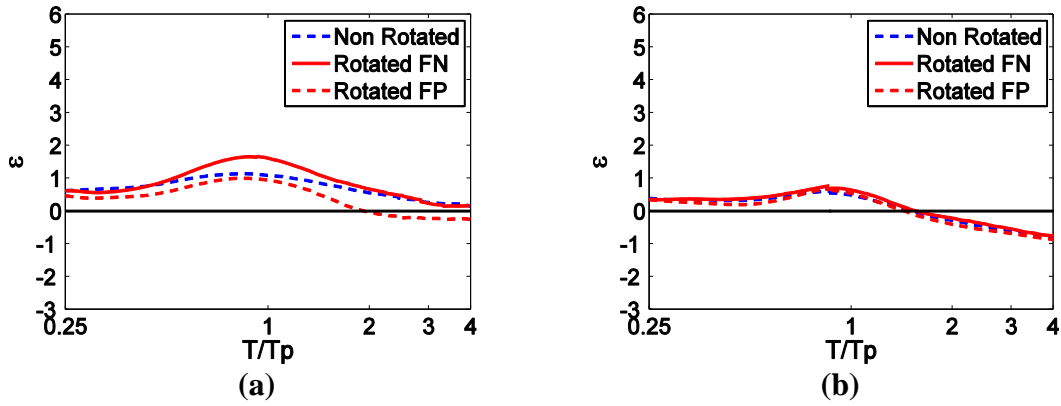

Figure 3. Average ε values for ground motions where FN is pulse-like (a) and non-pulse-like (b).

---

[2] The GMPE in [11] uses GMRotI as the IM (the 50th percentile of the geometric means of spectral accelerations computed for all non-redundant rotation angles of horizontal 2-component ground motion). GMRotI was used herein for the non rotated records; for FN and FP components the elastic spectral acceleration, $S_{a,e}(T)$, was used as the IM while, in principle, the GMPE should be transformed consistently (see [12] for a discussion). All the parameters required to compute the GMPE were available for the considered records via the NGA flatfile (http://peer.berkeley.edu/assets/NGA_Flatfile.xls).

[3] A small bump trend may be observed also in the non-pulse-like records. This is believed to be related to the fact that these records, for which a pulse period was always identified by Baker [8], may have a pulse feature of some significance (e.g., from site effects or other factors) which the plot in terms of T/Tp magnifies.

It is to note that quantifying ε for pulse-like records allows to account for the peculiar spectral shape modifying ordinary GMPEs without requiring to fit a specific one. In this direction, Baker [10] proposed a modification factor for an existing GMPE (calibrated on that of Boore and Atkinson [11]):

$$\overline{\overline{\ln\left(S_{a,e}\left(T\right)\right)}} = \overline{\ln\left(S_{a,e}\left(T\right)\right)} + e^{-\left(\ln\left(T/T_p\right)\right)^2} \tag{2}$$

where $\overline{\overline{\ln\left(S_{a,e}\left(T\right)\right)}}$ is the predicted spectral acceleration modified for pulse-like features in ground motion the last term in the right hand side models the bump[4] of spectral ordinates with a maximum at T equal to Tp. This will be applied in section 3.3 to a GMPE for Italy and to ground motion records of L'Aquila earthquake. In general it may be used to adjust probabilistic seismic hazard analysis to account for near-source effects [9,14].

2.2 Integral parameters of ground motions

Two integral ground motion intensity measures were also computed for the NGA records to see whether there are significant near-source effects on signals' *duration*: the Arias intensity (A_I), and the significant duration (S_D) [15]. Table 3 shows the medians and the differences between 25th and 75th percentiles of the empirical distributions (range), both being robust statistical estimators.

Table 3. Integral IMs.

Type		Sample Size	A_I [cm/sec]		S_D [sec]	
			Median	Range	Median	Range
Pulse-Like	FN	73	0.09	0.15	8.42	5.82
	FP	73	0.07	0.13	9.10	5.12
Non-Pulse-Like	FN	289	0.04	0.09	10.93	6.58
	FP	289	0.04	0.08	11.10	6.69

A_I is a measure of energy; i.e., it is function of event magnitude, source-to-site distance and soil conditions, it can be used only to compare the same signals differently rotated. It is expected that, for pulse-like records, the A_I FN/FP ratio is systematically higher than one because FN is more energetic (see section 2.1). In fact, ratios of medians are 1.23 (with standard deviation equal to 0.63) and 1.07 (with standard deviation equal to 0.57) for pulse-like and non-pulse-like, respectively.

$\quad$ S_D is the time in which the ground motion releases 90% of its total energy, and it may be used to compare signals from different sites and earthquakes. It is expected that pulse-like signals have a significant duration lower than non-pulse-like. Values in Table 3 seem to qualitatively[5] confirm it with median values of 8.42 versus 10.93 for the FN

---

[4] Note that this modification of attenuation may be considered as a *narrow band* one [13]; i.e., elastic demand is magnified for selected frequency corresponding to the pulse period. Former models to modify ordinary GMPEs to account for directivity are *broad band*; e.g., that of Somerville et al. [1].

[5] Statistical tests on integral parameters distributions would be useful to confirm or not these comparisons, but the large sample sizes and asymmetric shape distributions (see Figure 4) suggest that the most parametric tests would not be useful, while non-parametric are not as powerful.

components of pulse-like and non-pulse-like records, respectively. Figure 4 shows the histograms of A_I (a) and S_D (b) and their median values (vertical dashed lines).
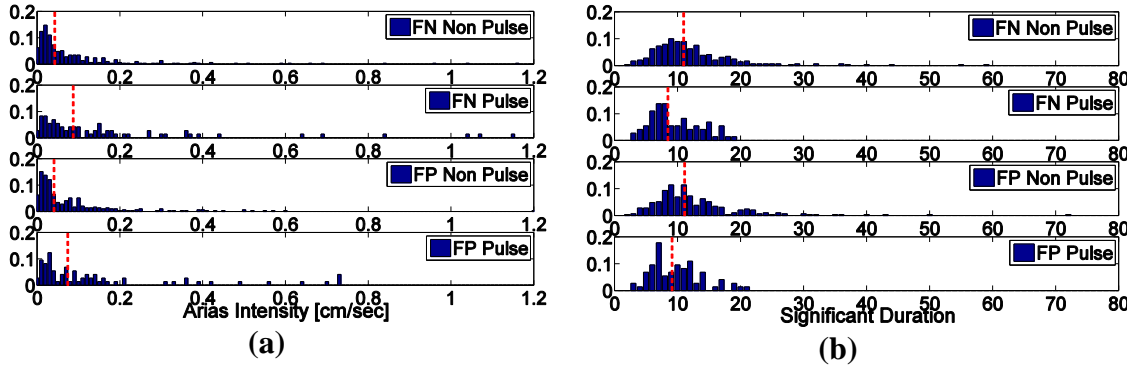

Figure 4. Arias Intensity (a) and Significant Duration (b) histograms for NGA records.

2.3 Inelastic demand and displacement amplification factor

In order to analyze pulse-like effects on non-linear structures, bilinear single degree of freedom (SDoF) systems, with 3% hardening ratio, 5% damping ratio, and different values of the strength reduction factor (R_s), Equation (3), were considered.

$$R_s = S_{a,e}(T) \cdot m / F_y \qquad\qquad (3)$$

In Equation (3) T is the oscillation period of the SDoF; m is its mass; and F_y is its yielding strength.

From this analysis there is the evidence that, also in the non-linear case, the FN over FP ratio is comparatively larger for those records in which the fault-normal component is identified as pulse-like with respect to ground motions where FN is non-pulse-like (Figure 5a, b and c). Ranges of the FN over FP ratio are 1.39÷1.67, 1.20÷1.54 and 1.40÷1.72 for R_s equal to 2, 4 and 6, respectively. Moreover, as a consequence of the peculiar spectral shape observed in section 2, unexpected displacement demand may occur in structures having non-linear oscillations in a period range around to that of the pulse. A way to visualize this is a plot of the logarithm of the inelastic ($S_{d,i}$) to elastic ($S_{d,e}$) displacement ratio of the bilinear SDoF systems already described. Figure 5d, e and f, report, for the three R_s values, the averages for: FN and FP components of ground-motions where FN is pulse-like (*Pulse - Fault normal* and *Fault Parallel* in the legend), and for non-pulse-like FN components (*Non Pulse - Fault normal* in the legend). These latter records are considered ordinary and, therefore, are used as a benchmark. The FP components of ground-motions where FN is non-pulse-like were not plotted as their curve perfectly overlaps with that of FN (as the ε plots of Figure 3b suggest).

Curves for the FN pulse-like records show an increment in the $S_{d,i}/S_{d,e}$ ratio at $T/T_p \approx 0.3÷0.5$, indicating a comparatively larger inelastic demand of this kind of near-fault ground motions because the elongated structural period drifts toward the peak at the pulse period Tp [16].

FP components of records where FN is pulse-like show a lower increment with respect to FN, nevertheless it is not perfectly overlapping with that of ordinary records. This is expected to some extent because, as discussed, in the strike-parallel direction

directivity effects are lower than in fault-normal direction, but they seem to be not absent (see [5] for a discussion about nature and seismic demand of FP-rotated near-source records).
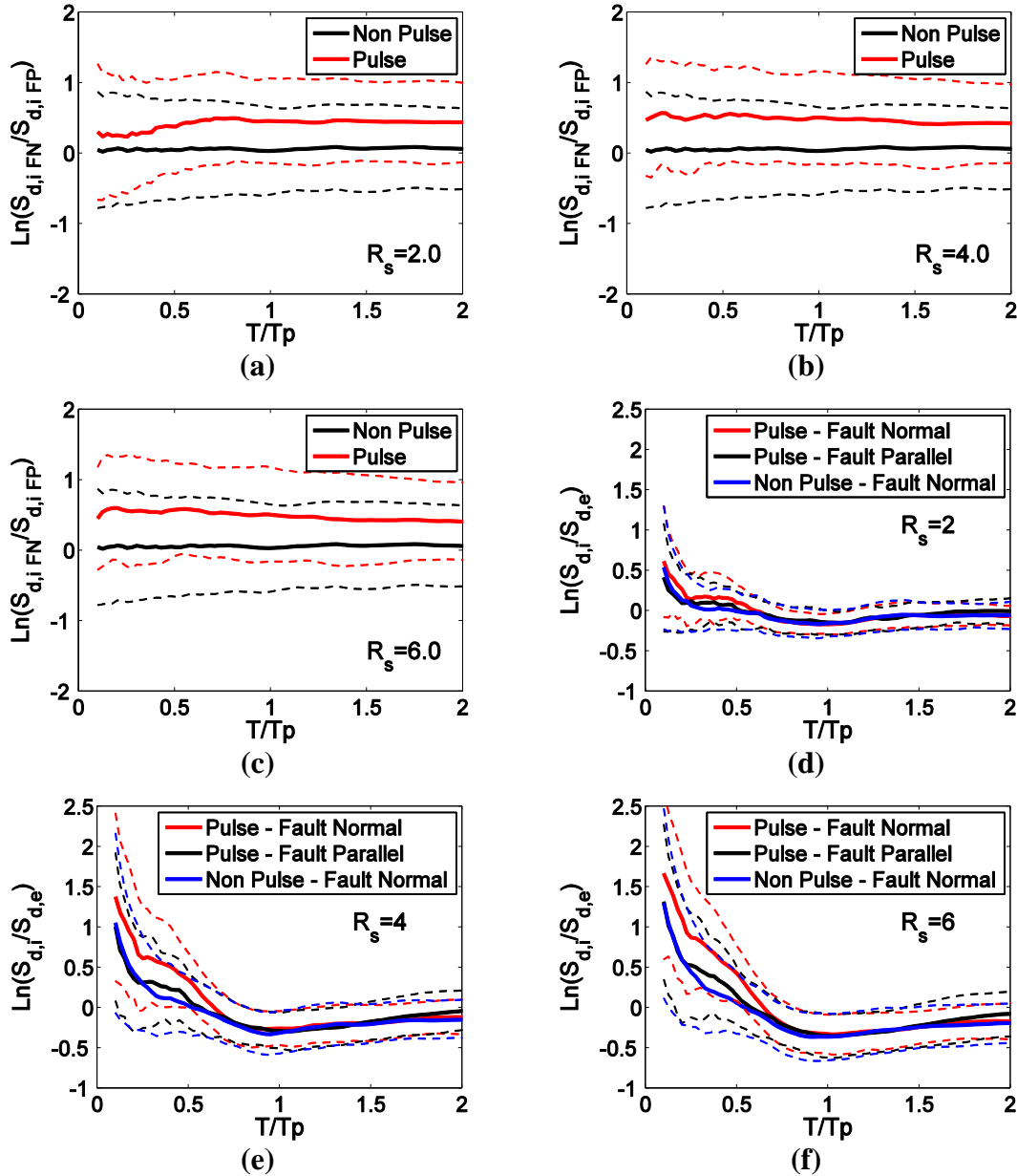

Figure 5. FN over FP inelastic displacement ratios (a, b and c) and inelastic to elastic displacement demand ratios (d, e, and f).

To quantify what derived from Figure 5, Table 4 reports the maxima of the increments in the $S_{d,i}/S_{d,e}$ ratio of FN pulse-like with respect to FN non-pulse-like records for the three R_s values. More precisely, Table 4 shows T/T_p and $S_{d,i}/S_{d,e}$ median ratios for pulse-like ground-motions in FN and FP directions and $S_{d,i}/S_{d,e}$ ratios for FN non-pulse-like records. In FN direction the increments of the pulse-like with respect to the non-pulse-like are equal to 18%, 53% and 71% for R_s equal to 2, 4 and 6, respectively. Increments of the same for ratio, for FP components of records where FN is pulse-like with respect to non-pulse-like FN ground motions, are equal to 9%, 15% and 21%. As a consequence of these increments, inelastic to elastic ratio is not similar to that of

ordinary records; i.e., it may violate the *equal displacement rule* and therefore should be accounted for properly in seismic design and assessment.

Table 4. Values of $S_{d,i}/S_{d,e}$ ratios corresponding to maximum increment for FN pulse-like with respect to FN non-pulse-like.

	T/Tp	Pulse - FN	Pulse - FP	Non Pulse - FN
$R_s = 2$	0.325	1.196	1.104	1.015
$R_s = 4$	0.350	1.738	1.304	1.133
$R_s = 6$	0.325	2.182	1.543	1.278

3 NEAR-SORCE EFFECTS IN THE APRIL 6TH 2009 L'AQUILA EARTHQUAKE

In this section pulse-like effects in seismic action are discussed for the M_w 6.3 April 6 mainshock of the L'Aquila earthquake sequence. In particular: (i) the information about the source of the earthquake and recording sites within about 30 km in terms of closest distance to fault rupture is reviewed; (ii) near-source records are rotated in terms of FN and FP directions, and the seismic action is analyzed comparing those signals in which velocity pulses are found to those non-pulse-like of the same event and to the NGA results; (iii) a model for the probability of occurrence of velocity pulses, based on the source/site geometry, is applied to the fault in question; (iv) finally, an analysis including the vertical component of ground motions is shown.

3.1 Near-source features

Results of seismological studies have shown that the Abruzzo event was a *normal* faulting earthquake (or *dip-slip*), with a rectangular rupture plane of about 17x14km^2 and located at a depth between 12 km and 0.6 km from the surface. The rupture plan has a strike of 142°, a dip of 50° and a rake of 90° (D. Cheloni[⊥], written communication). Coordinates of the vertices of the rupture plane and of the hypocenter are reported in Table 5. These data are not uniquely identified by all seismologists, but the various available estimates are not very different each other. Propagation of the rupture seems to have occurred *up-dip* first, and then in the direction parallel to the strike.

Table 5. Hypocenter and rupture plane coordinates.

	Fault Plane Vertices				Hypocenter
Longitude	13.424°	13.552°	13.465°	13.336°	13.353°
Latitude	42.405°	42.293°	42.238°	42.351°	42.340°
Depth (km)	0.600	0.600	11.800	11.800	11.800

The mainshock was recorded by the stations of the National Accelerometric Network (RAN) of the Italian Civil Protection, whose raw data are available at http://www.protezionecivile.it/. Figure 6 shows the projection of rupture surface with

---

[⊥] Istituto Nazionale di Geofisica e Vulcanologia (INGV), Centro Nazionale Terremoti (CNT), Rome, Italy.

the epicentral location, the code of RAN stations[6], their Eurocode 8 (EC8) [18] site class [19], and some severely damaged towns and villages [20].

The acceleration waveforms were corrected by the authors in terms of linear baseline correction and Butterworth Bandpass filter (low-cut = 0.1 Hz, high-cut 2 = 25 Hz, order = 4). It is to recall that some authors [21] have discussed how a constant cut-off filter may affect the long-period components of the ground motions and therefore it may be conservative for some of the records used in this article; further details on the corrected signals, which are available at http://www.reluis.it/, may be found in [22].

The horizontal components of each record were also rotated from North-South (N-S) and East-West (E-W) (original directions of accelerometers) to FN and FP directions (strike-normal and strike-parallel components). All analyses of horizontal components will be referred to FN- and FP-rotated signals unless otherwise specified.

In this work, only stations with fault distance within about 30 km (13 in number) were considered because this is a generally accepted (although arbitrary) boundary for near-source effects. Table 6 shows some peak and integral intensity measures of recorded ground motions at the near-source stations; i.e., PGA, Peak Ground Velocity (PGV), Peak Ground Displacement (PGD), A_I, and the Cosenza and Manfredi Index (I_D) [23], S_D and Bracketed Duration at 5% PGA (B_D) [15].
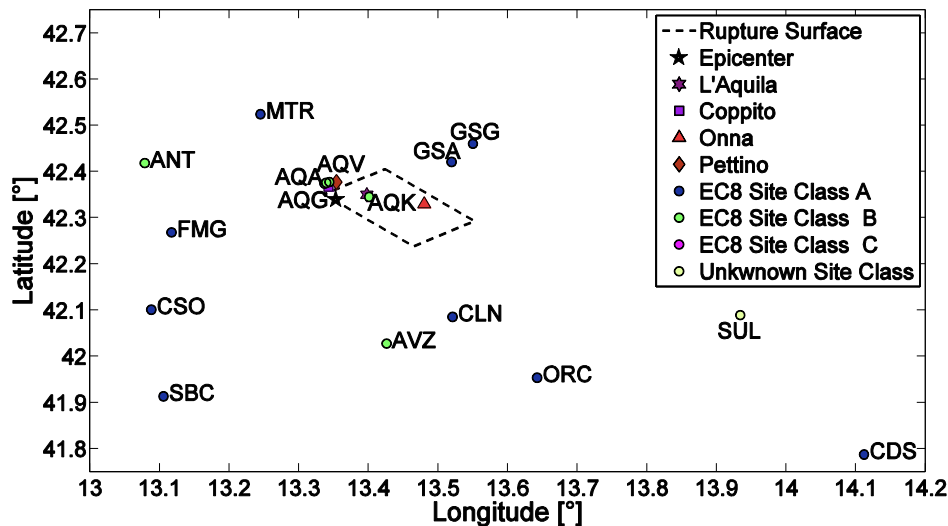

Figure 6. Map view of rupture surface and RAN accelerometric stations within about 60 km from the fault projection.

Table 6. Peak and integral IMs of L'Aquila near-source records.

	Record	PGA [cm/sec^2]	PGV [cm/sec]	PGD[7] [cm]	A_I [cm/sec]	I_D [-]	S_D [sec]	B_D [sec]
1	AQV_FN	725.37	37.63	5.53	228.76	5.24	7.69	25.14
	AQV_FP	474.42	31.41	7.07	253.90	10.64	7.61	66.41
2	AQG_FN	357.16	34.08	8.19	114.47	5.88	8.16	18.23
	AQG_FP	391.79	26.60	5.45	144.91	8.68	8.45	25.17

---

[6] All the analyses discussed in the following do not attempt to account for other near source effects which may cause spatial variability of ground motions; e.g., hanging/foot wall effects [17]. This is also because most of near source stations lie on the hanging wall.

[7] Note that PGD is especially sensitive to the low-cut filter, therefore the reliability of listed PGD values is confined to the implemented filtering methodology.

3	AQA_FN	425.86	28.67	7.11	132.60	6.79	6.91	14.78
	AQA_FP	404.55	19.91	3.32	198.89	15.50	7.72	67.33
4	AQK_FN	413.57	45.01	13.22	138.10	4.63	10.55	66.06
	AQK_FP	261.99	16.66	5.32	81.96	11.73	15.37	66.51
5	GSA_FN	153.52	10.91	3.35	37.13	13.86	9.38	25.53
	GSA_FP	197.58	6.02	1.37	46.50	24.48	8.02	24.10
6	CLN_FN	99.54	5.48	1.76	3.87	4.43	8.00	20.05
	CLN_FP	63.29	5.82	2.26	3.75	6.37	6.53	19.13
7	AVZ_FN	61.91	13.06	3.40	8.43	6.51	21.56	51.28
	AVZ_FP	63.41	9.89	3.54	9.14	9.10	18.25	49.76
8	MTR_FN	51.04	4.08	0.93	4.02	12.04	14.84	45.93
	MTR_FP	57.19	3.04	0.88	5.17	18.59	11.39	34.84
9	GSG_FN	20.31	3.66	2.14	0.81	6.81	10.65	33.28
	GSG_FP	25.52	2.31	0.71	0.69	7.33	10.97	25.59
10	FMG_FN	21.87	2.12	0.98	1.34	18.12	22.76	60.38
	FMG_FP	24.43	1.90	0.92	0.88	11.87	20.58	41.78
11	ANT_FN	26.66	2.25	0.47	1.67	17.33	21.68	54.48
	ANT_FP	19.19	1.99	0.43	0.96	15.74	22.87	64.52
12	CSO_FN	18.91	2.24	1.00	0.89	13.11	21.38	58.06
	CSO_FP	13.74	1.48	0.43	0.48	14.74	27.23	65.69
13	ORC_FN	72.64	6.88	1.11	4.77	5.97	10.24	30.10
	ORC_FP	31.85	2.86	0.99	1.83	12.60	14.00	50.95

3.2 Looking for pulse-like records

The algorithm developed by Baker [8] calculates, for each record, a score called *pulse indicator*. Records with score above 0.85 and below 0.15 are classified as pulses and non-pulses respectively, while signals with a score between these limits are considered *ambiguous*. Two further conditions are added in order to exclude pulse-like signals likely to not be related to directivity. The first one is that records with a pulse not occurring at the beginning of the record (i.e., *late* pulses) are not considered to be affected by directivity, the second one refers to PGV that has to be higher than 30cm/sec; this is claimed to exclude records with poor structural interest. In this work, this latter condition is neglected consistently with [9].

The procedure to identify pulses has been implemented by J.W. Baker[*] in some MATHWORKS-MATLAB® scripts and is publicly available at http://www.stanford.edu/~bakerjw/pulse-classification.html (last accessed January 2009). It was used to analyze L'Aquila records; Table 7 shows the results of pulse identification for the records of Table 6; identified pulse-like records are reported in bold. Thirteen stations were analyzed and six of them have a horizontal component classified as pulse-like: 5 of them in the FN direction and only one in the FP direction, AQV. The latter one has also the FN component classified as ambiguous and the elastic displacement spectra are similar in the two analyzed directions. The choice of

---

[*] Stanford University, CA, US.

neglecting the PGV limit significantly affects only the two results of GSG[8] (PGV equal to 3.66cm/sec) and ORC (PGV equal to 6.88cm/sec).

Table 7. Results of pulse identification for horizontal components.

Component	Pulse indicator	Late pulse indicator	PGV [cm/sec]	Classified as Pulse	Tp [sec]
AQV_FN	0.70	0.00	37.63	NO	0.53
AQV_FP	**0.85**	**0.00**	**31.41**	**YES**	**1.06**
AQG_FN	**1.00**	**0.00**	**34.08**	**YES**	**1.02**
AQG_FP	0.71	0.00	26.60	NO	1.11
AQA_FN	**0.93**	**0.00**	**28.67**	**YES**	**0.74**
AQA_FP	0.00	0.00	19.91	NO	0.62
AQK_FN	**1.00**	**0.00**	**45.01**	**YES**	**1.99**
AQK_FP	0.00	1.00	16.66	NO	1.26
GSA_FN	**0.72**	**0.00**	**10.91**	**YES**	**3.13**
GSA_FP	0.00	0.00	6.02	NO	1.97
CLN_FN	0.05	1.00	5.48	NO	5.17
CLN_FP	0.01	1.00	5.82	NO	4.81
AVZ_FN	0.97	1.00	13.06	NO	1.88
AVZ_FP	0.00	1.00	9.89	NO	1.61
MTR_FN	0.01	1.00	4.08	NO	2.60
MTR_FP	0.00	1.00	3.04	NO	2.16
GSG_FN	**0.95**	**0.00**	**3.66**	**YES**	**4.03**
GSG_FP	0.08	1.00	2.31	NO	5.17
FMG_FN	0.00	1.00	2.12	NO	4.03
FMG_FP	0.01	0.00	1.90	NO	4.76
ANT_FN	0.00	0.00	2.25	NO	0.95
ANT_FP	0.00	0.00	1.99	NO	2.76
CSO_FN	0.00	1.00	2.24	NO	4.82
CSO_FP	0.00	1.00	1.48	NO	2.22
ORC_FN	**0.92**	**0.00**	**6.88**	**YES**	**0.83**
ORC_FP	0.00	1.00	2.86	NO	4.47

Figure 7 shows an example of the algorithm's output for a pulse-like station (AQK) with recorded velocity, extracted pulses, residual signals and displacement time histories. FN and FP components are reported on the left and right panels, respectively. The former is pulse-like with score 1, and the latter is non-pulse-like with score 0.0. AQK is the stations with the strongest pulse-like signal in FN direction[9].

Studying ambiguous cases, authors have decided to classify as pulse-like also the FN signal of GSA. Elastic displacements spectra seem to confirm this choice (see the following section). All the other ambiguous cases were considered as non-pulse-like.

---

[8] GSG station seems, according to [19], to be in tunnel 200m below the surface. Nevertheless, it was kept in the analyses also because it was found that removing it would not change the conclusions found.

[9] It is to report, however, that Paolucci [24] argues it may derive also from a site effect in combination with the source radiation.
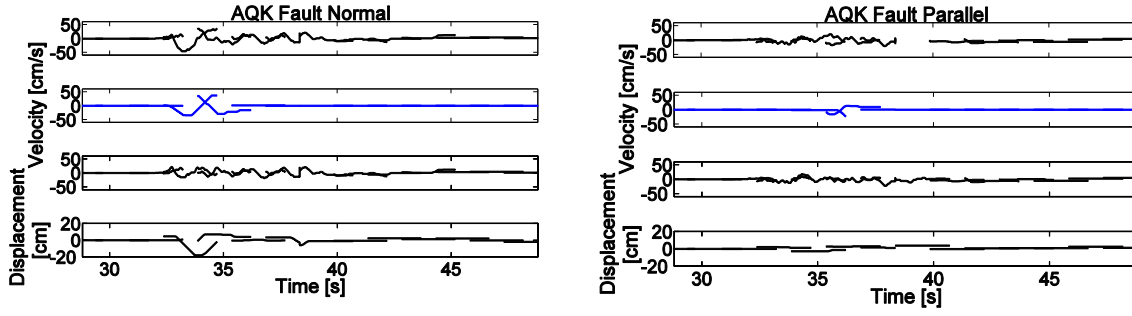
Figure 7. From the top to the bottom: velocity time-history, extracted pulse, residual velocity, and displacement signal for FN (left) and FP (right) component of AQK.

A model for the prediction of the pulse occurrence, $P\left[pulse\right]$, developed for PSHA purposes [9] on the basis of the parameters indicated by Somerville et al. [1], was applied to the fault of the earthquake as it may be useful to assess if pulses occurred where the geometrical source-to-site configuration favors it. The parameters, in the case of dip-slip faults (see Figure 8), are: the closest distance to fault rupture (Clstd or R); the fraction of the rupture surface that lies between the hypocenter and the site (d); the angle between the direction of rupture propagation and the direction aligning the hypocenter and the site (φ). The considered model, Equation (4), was obtained via logistic regression and is applicable for the 5km÷30km, 0km÷20km, 0°÷90° ranges of R, d, and φ, respectively.

$$P\left[pulse\middle|R,d,\varphi\right]=\frac{e^{0.553-0.055\cdot R-0.0267\cdot d-0.027\cdot\varphi}}{1+e^{0.553-0.055\cdot R-0.0267\cdot d-0.027\cdot\varphi}} \tag{4}$$

Figure 8 shows schematically the geometrical predictors for three different cases of relative rupture-site position in the L'Aquila earthquake. The zones' definition refers to what is depicted in Figure 9: in case 0 φ is larger than 90°, while cases 1 and 2 only differ because of the geometrical relationship between the three parameters for predicting probability. Figure 9 shows the probability contours according to the model.
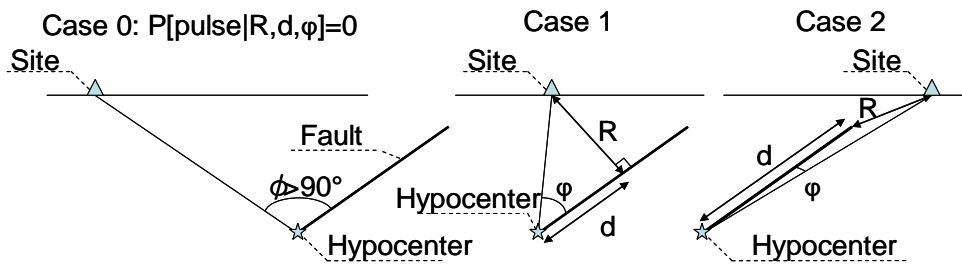

Figure 8. Geometrical predictors for three different cases of relative rupture-site position.

Table 8 shows values of geometrical predictors and pulse occurrence probability for the near-source stations. It is to point out that the occurrence probability is never larger than 0.5; this is because the model was developed generically for non-strike-slip earthquakes, which are often complex and in which it is not easy to identify rupture directivity effects. Nevertheless, it may be used to highlight sites comparatively more likely to be affected by velocity pulses given the source geometry. From this point of view, results of pulse

occurrence probability model are in general agreement (except ORC) with the results of algorithm for pulse-like identification[10].
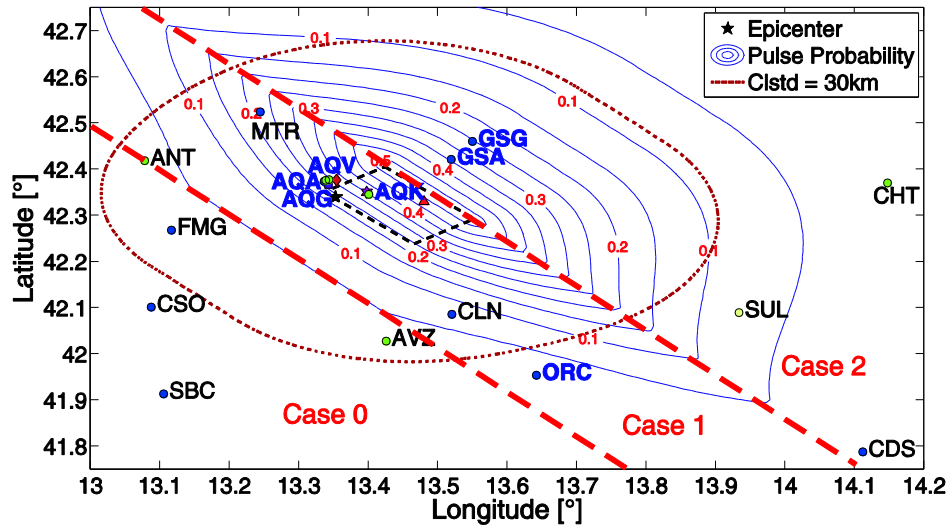

Figure 9. Contours of occurrence probability and accelerometric stations with pulse-like signals (blue).

Table 8. Geometrical predictors and pulse occurrence probability for each accelerometric station.

Station	Long.	Lat.	R (km)	d (km)	φ (deg)	P[pulse]
AQV	13.34°	42.38°	6.07	10.16	29.60	0.30
AQG	13.34°	42.37°	6.60	9.70	33.05	0.28
AQA	13.34°	42.38°	6.41	9.85	31.71	0.28
AQK	13.40°	42.34°	4.80	10.94	23.69	0.34
GSA	13.52°	42.42°	7.14	14.21	14.79	0.35
CLN	13.52°	42.09°	20.77	3.78	74.13	0.06
AVZ	13.43°	42.03°	26.48	0.00	0.00	0.00
MTR	13.24°	42.52°	19.73	12.97	10.67	0.24
GSG	13.55°	42.46°	11.89	14.21	21.31	0.26
FMG	13.12°	42.27°	23.47	0.00	0.00	0.00
ANT	13.08°	42.42°	25.37	1.29	85.47	0.04
CSO	13.09°	42.10°	35.62	0.00	0.00	0.00
ORC	13.64°	41.95°	36.66	2.69	79.80	0.02

3.3 Seismic action

In order to further confirm the identification of pulse-like records and to see whether they are of special interest for structural engineering because carrying non-ordinary seismic demand, a comparison of seismic action was carried out with NGA records. First of all, the extracted Tp values were compared to the expected pulse period distribution computed via a period versus magnitude regression calculated on the NGA record dataset, although several others are available in literature [13,8]. Equation 5,

---

[10] It is to mention, for completeness, that seismologists [19] identify directivity in the comparatively large PGA values observed along the S-E quadrant of Figure 6, although it is still controversial whether this may be because some geological futures favoring the propagation in this direction and whether directivity, as described at the beginning of the paper, may be found simply analyzing PGA.

gives the natural logarithm of Tp as a function of M_w with a standard deviation of the residuals equal to 0.59. Figure 10 shows a plot of Equation (5) (solid line is the average, while dashed are plus and minus standard deviation of the residuals) and L'Aquila data.
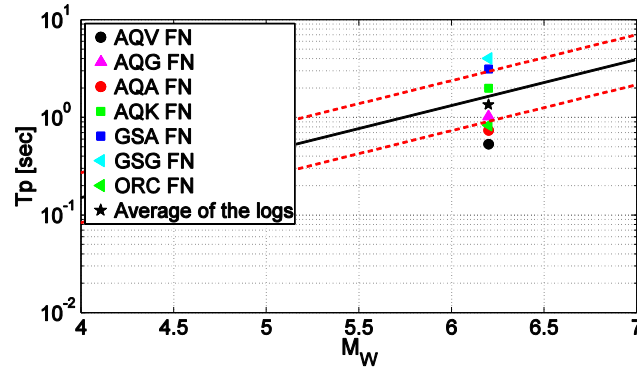
$$\ln Tp = -6.19 + 1.07 \cdot M_W \tag{5}$$

Figure 10. Comparison between extracted L'Aquila pulse periods and predicted values by regression of NGA data.

In Figure 11, elastic displacement spectra of pulse-like stations are shown as a function of T normalized with respect to Tp. T over Tp ratio takes values between 0.1 and 2.0 and spectra are computed with steps of 0.025 sec. Signals are grouped as FN and FP, then in the first plot (left) there are 6 pulse-like records and one non-pulse-like record (classified as ambiguous)[11].

The two components of AQV signals are very similar to each other; this is an expected result from the scores given by the algorithm. Moreover the figures show that the FN component of GSA is significantly different from FP. This is in good agreement with the choice of the authors about pulse classification of this station.

To quantify how much the FN components are stronger than the corresponding FPs, Figure 12 shows the averages of the natural logarithm of elastic and inelastic spectral displacement ratios. Comparing Figure 12 with Figure 5a, b and c, it is to note that trends are similar to NGA results. Maximum values of FN over FP ratio are 1.71, 1.70, 2.10 and 1.98 respectively for R_s equal to 1, 2, 4, and 6.

---

[11] Because L'Aquila downtown FN record (AQK station) is clearly stronger than all others, to ensure robustness of results, all following considerations will be referred to the median values, as it is more robust then mean with respect to outliers.
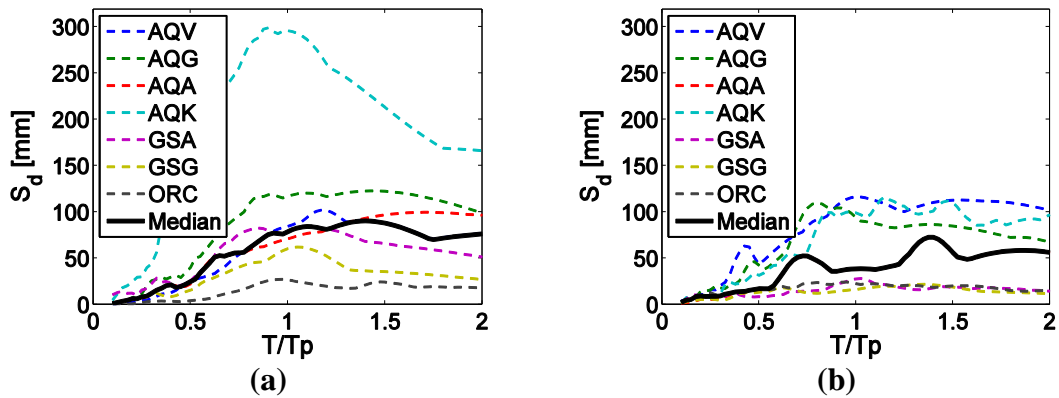
Figure 11. Elastic displacement spectra of pulse-like stations: (a) FN and (b) FP components.
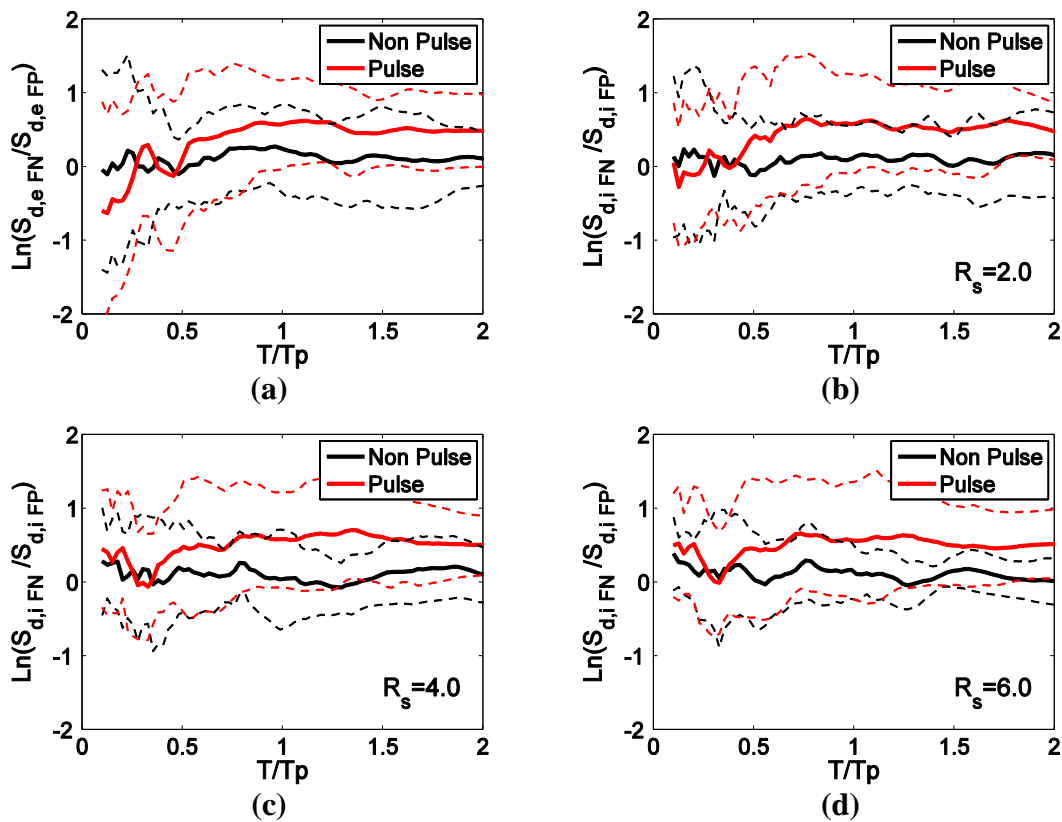

Figure 12. FN over FP elastic (a) and inelastic (b, c and d) displacement ratio for R_s = 2, 4 and 6.

Figure 13 shows the inelastic to elastic displacement ratios versus the oscillator period divided by Tp. Plots, calculated for three R_s factors, are compared to NGA FN records. Although the small sample size, L'Aquila displacement ratios have shapes very similar to the NGA results for stations without pulse-like effects. Also results for pulse-like stations agree to what expected although also the FP signals seem to be severe.
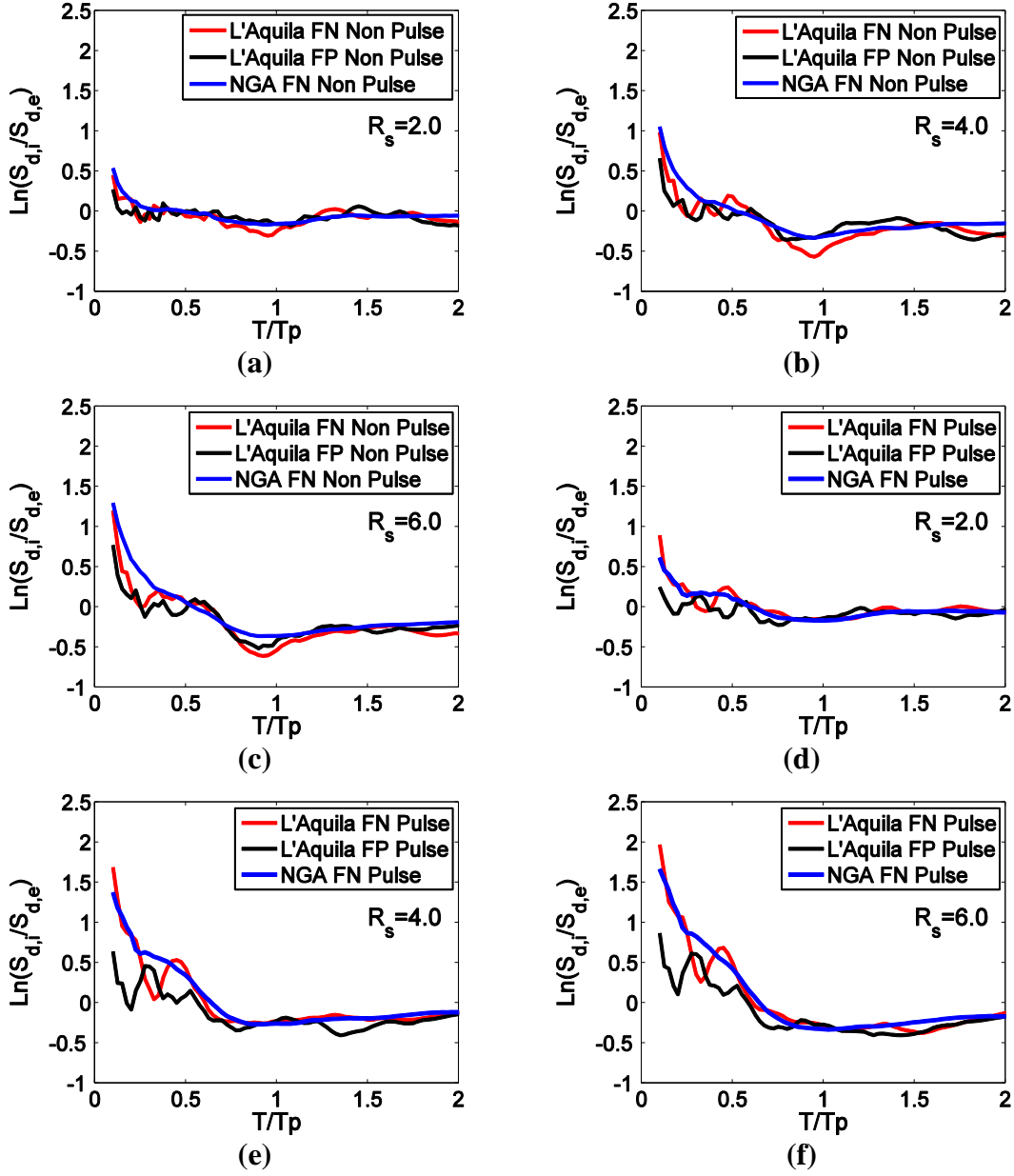
Figure 13. a, b and c - Inelastic to elastic displacement demand ratio for $R_s = 2$, 4 and 6 for non-pulse-like stations; d, e and f - Inelastic to elastic displacement demand ratio for $R_s = 2$, 4 and 6 for pulse-like ground motions.

As done for the NGA records, ε values were calculated for pulse-like and non-pulse-like L'Aquila FN components with respect to a GMPE, that is, the Sabetta and Pugliese attenuation law [25], which is built on the largest horizontal component of Italian strong-motion data. The GMPE was preliminarily modified to remove the event bias on the mean. To this aim, a factor, $\alpha(T)$ was added to the GMPE[12]:

---

[12] In the application of the attenuation relationship [25], the surface wave magnitude (M_s) value of the L'Aquila earthquake is assumed to be the same as the M_w value.

$$\overline{\log_{10}\left(S_{a,e}\left(T\right)\right)} = \log_{10}\left(a + b\cdot M + c\cdot\log_{10}\left(R_{epi}^2 + h^2\right)^{\frac{1}{2}} + e_1\cdot S_1 + e_2\cdot S_2\right) + \alpha\left(T\right) \tag{6}$$

where $\overline{\log_{10}\left(S_{a,e}\left(T\right)\right)}$ is the value of spectral acceleration obtained by the modified attenuation relationship; a, b, c, h, e_1, e_2, are the coefficients of the original attenuation relationship which depend on T and allow to account for magnitude (M), epicentral distance (R_{epi}), and site conditions and are equal to 1 for shallow and deep alluvium sites, respectively, and 0 otherwise; and $\alpha\left(T\right)$ is given in Equation (7) being computed using only of the spectral acceleration values of the FN components of near-source ground motions classified as non-pulse-like (i.e., those supposed to be ordinary).

$$\alpha\left(T\right) = \frac{1}{6}\sum_{i=1}^{6}\log_{10}\left(S_{a,e}\left(T\right)\right)_i - \log_{10}\left(a + b\cdot M + c\cdot\log_{10}\left(R_{epi}^2 + h^2\right)^{\frac{1}{2}} + e_1\cdot S_1 + e_2\cdot S_2\right)_i \tag{7}$$

The intra-event standard deviation $\sigma\left(T\right)$ (base 10 logarithms) also was estimated as the standard deviation of the residuals of non-pulse-like FN components within 30 km. Numerical values of α and σ are reported in Table 9 for each oscillation period T.

Table 9. Values of $\alpha\left(T\right)$ and $\sigma\left(T\right)$ for each period

T (sec)	0	0.04	0.07	0.1	0.15	0.2	0.3	0.4	0.5	0.75	1	1.5	2	3.03	4
α	-0.4	-0.4	-0.4	-0.4	-0.5	-0.4	-0.5	-0.4	-0.4	-0.4	-0.3	-0.3	-0.3	-0.3	-0.1
σ	0.3	0.4	0.4	0.3	0.3	0.3	0.3	0.2	0.2	0.2	0.2	0.5	0.3	0.4	0.4

Figure 14a shows average ε values, computed after modification, for FN and FP components of pulse-like ground motions. In the same figure, ε values of average non rotated (N-S and E-W) horizontal components of the stations which have recorded pulses are also reported. As shown for the NGA data, rotated and non rotated ε have the same shape, with the non rotated values in an intermediate position between FN and FP values. It has to be highlighted that ε values of non rotated and FP records were computed with the attenuation law modified with respect to FN components of non-pulse-like ground motions and using the estimated $\sigma\left(T\right)$ values. In Figure 14b, the ε values of FN components of pulse-like records are given considering the modification of Equation (2) accounting for the peculiar spectral shape of pulse-like records; i.e., Equation (8). In the same figure also ε values of FN components of non-pulse-like records are reported (in this latter case ε is computed only with the modification of the GMPE according to Equation (6)).

$$\overline{\ln\left(S_{a,S\&P}\left(T\right)\right)} = \left(\log_{10}\left(e\right)\right)^{-1}\cdot\overline{\log_{10}\left(S_{a,e}\left(T\right)\right)} + e^{-\left(\ln\left(T/T_p\right)\right)^2} \tag{8}$$

Because, the Sabetta and Pugliese relationship is not valid for T larger than 4s, the ε values for all records with Tp larger 1 sec cannot be represented entirely in the 0÷4 T/Tp range, this is why the plot in Figure 14 has unexpected trend for high T over Tp ratio; i.e., the average plotted corresponds to a single record.
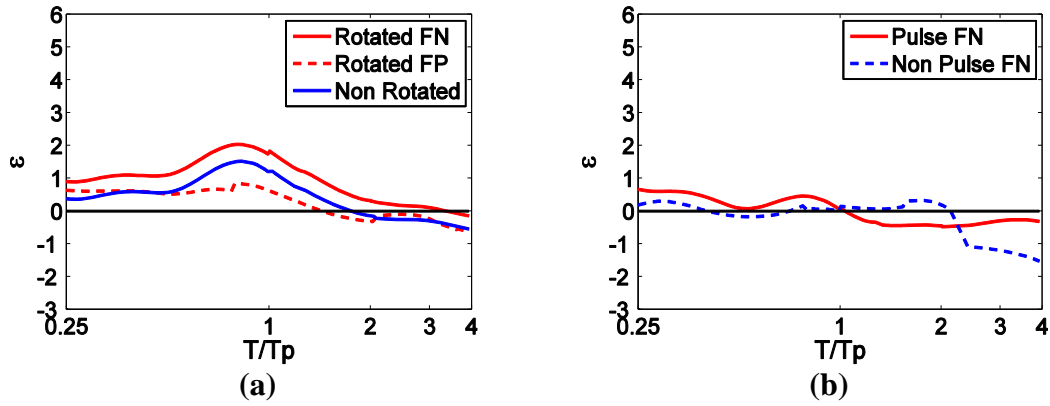
Figure 14. (a) Average ε values of L'Aquila pulse-like records; (b) Average ε values for FN components of L'Aquila pulse-like and non-pulse-like records with modified attenuation relationship.

4   UN-ROTATED RECORDS

In accordance with all models used and suggested by literature, only horizontal FN- and FP-rotated components were analyzed so far. Similar analysis of the un-rotated components seems to confirm that the rupture directivity effects have to be studied in FN and FP components as:

1. In the case of pulse-like signals, FN direction has seismic displacement demand higher than the other two un-rotated components. Conversely, the FP direction identifies the lowest seismic demand. This is briefly shown in Figure 15a where the means of the logarithms of rotated over un-rotated (N-S and E-W) spectral ratios for pulse-like ground motions are given. In the 0 sec to 3.0 sec interval, FN to EW and FN to NS average ratios are respectively equal to 1.12 and 1.32 respectively. Similarly FP to EW and FP to NS have average values of 0.80 and 0.91, respectively. Conversely, if non-pulse-like stations are analyzed, rotation does not affect the results, this is shown by Figure 15b. Same average values are reported for non-pulse-like stations, in this case the ratios are equal to 1.17 and 1.10 (FN/EW and FN/NS) or 1.05 and 0.89 (SP/EW and FP/NS). Similar results were observed by means of ε for NGA records in section 2.1;

2. Processing un-rotated signals, pulses were found in both in N-S and E-W directions in an apparently non-systematical way. More specifically, 5 signals in E-W direction and 4 signals in N-S directions were classified as pulses. Components of CLN recording were both classified as pulses.
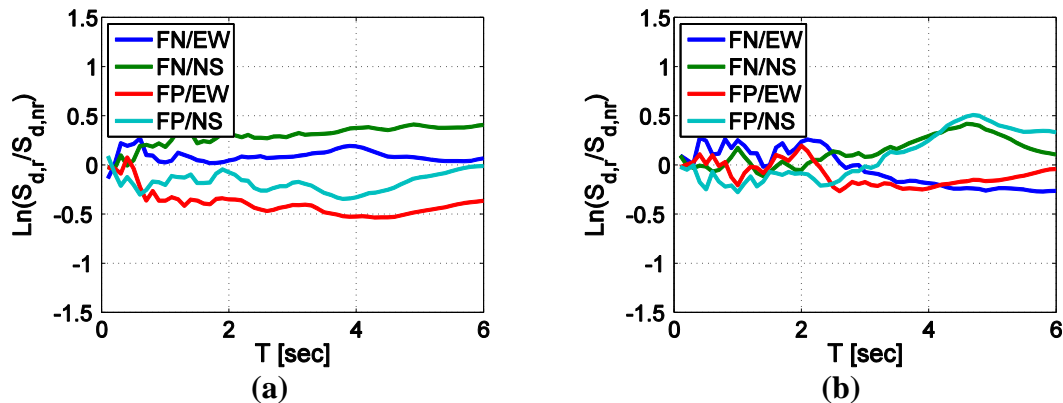

Figure 15. Rotated and non rotated elastic spectral displacement ratios for pulse-like (a) and non-pulse-

like records (b).

5   RUPTURE-NORMAL DIRECTION AND VERTICAL COMPONTENT

Finally, as suggested by [4], the horizontal strike-normal ground motion component was considered and analyzed as the fault-normal component. Strictly respecting the rupture geometry, the fault-normal direction is not horizontal for dip-slip earthquakes (Figure 1b), while it requires spatial rotation of the records, although authors were not able to find other studies addressing this same issue. Therefore, horizontal strike-normal rotated components were again rotated (including the vertical component) to obtain rigorous rupture-normal (RN) and rupture-parallel (RP) signals. However, analyzing the so-rotated records, Table 10, the picture is not as clear as in the case of strike-normal and strike-parallel rotation. In fact, pulse-like signals were identified both in RN and RP directions; i.e., 8 pulse-like signals are identified (reported in bold): 4 in RP and 4 in RN direction.

Table 10. Results of signals analyses for rupture-normal and rupture-parallel components.

Component	Pulse indicator	Late pulse indicator	PGV [cm/sec]	Classified as Pulse	Tp [sec]
AQV_RN	0.06	0.00	29.40	NO	0.55
AQV_RP	**1.00**	**0.00**	**26.62**	**YES**	**0.53**
AQG_RN	**1.00**	**0.00**	**31.89**	**YES**	**0.96**
AQG_RP	**0.93**	**0.00**	**16.67**	**YES**	**1.11**
AQA_RN	0.75	0.00	26.10	NO	1.11
AQA_RP	0.03	0.00	15.34	NO	1.74
AQK_RN	**1.00**	**0.00**	**42.33**	**YES**	**1.88**
AQK_RP	0.00	1.00	23.52	NO	1.70
GSA_RN	0.13	0.00	7.89	NO	3.02
GSA_RP	0.65	0.00	8.43	NO	3.28
CLN_RN	0.01	1.00	4.16	NO	5.40
CLN_RP	**1.00**	**0.00**	**6.83**	**YES**	**1.97**
AVZ_RN	0.94	1.00	11.45	NO	1.90
AVZ_RP	0.28	1.00	6.62	NO	1.65
MTR_RN	0.04	1.00	3.76	NO	2.98
MTR_RP	0.00	0.00	3.21	NO	3.06
GSG_RN	**0.99**	**0.00**	**4.13**	**YES**	**3.72**
GSG_RP	**1.00**	**0.00**	**2.85**	**YES**	**3.66**
FMG_RN	0.00	1.00	1.97	NO	3.44
FMG_RP	0.00	1.00	1.94	NO	1.59
ANT_RN	0.00	1.00	1.98	NO	2.32
ANT_RP	0.00	0.00	1.84	NO	0.92
CSO_RN	0.00	1.00	1.79	NO	5.51
CSO_RP	0.97	1.00	2.74	NO	3.97
ORC_RN	**0.98**	**0.00**	**7.01**	**YES**	**0.847**
ORC_FP	0.00	1.00	2.42	NO	4.746

Vertical components were also analyzed alone. Of the thirteen stations considered, the algorithm identifies only one vertical signal as pulse-like (CLN). To complete the study of vertical signals, average ε values were calculated for stations with pulse-like horizontal signals. In other words, also in this case the Sabetta and Pugliese GMPE [25] was modified to account for the average effect of the earthquake. In analogy with the horizontal case, stations without pulses (in the horizontal direction) were used to compute the vertical modification factor $\alpha(T)$. Results are plotted in Figure 16 showing that here is no significant trend and the absence of pulse-like effects seems to be confirmed.
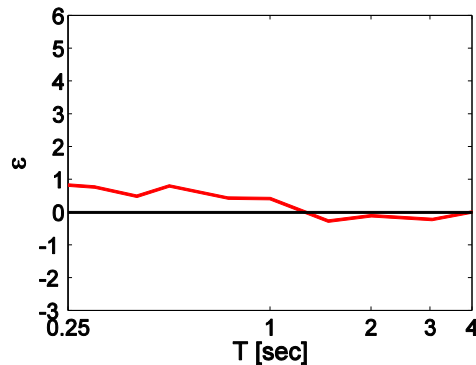

Figure 16. Average e values of vertical signals components of pulse-like stations.

6   CONCLUSIONS

Although the directivity-induced pulses problem is known since many years, a quantification of its significance for structural engineering and recognition of its occurrence in observed earthquakes is not well established yet. In this work, some recent tools to investigate pulse-like records were applied in order to analyze the issue as much as possible from a quantitative point of view and in terms of seismic action.

The amplification of elastic and inelastic seismic demands for pulse-like fault-normal records and the peculiar spectral shape driven by pulses were investigated first with respect to fault-parallel and non-pulse-like (ordinary) near-source ground motions. The dataset is a subset of FN- and FP-rotated records from the next generation attenuation project (NGA) database. Analyses show that pulse-like signals are characterized by fault normal records generally stronger than both fault parallel components and non-pulse-like ground motions. Moreover, fault-normal pulse-like signals are also characterized by a non-standard spectral shape with an increment of spectral ordinates in a range around the pulse period. Comparisons between pulse-like and non-pulse-like records show that inelastic to elastic seismic spectral displacement ratio for pulse-like records can be 20% to 70% higher than that of ordinary motions depending on the non-linearity level.

The results of the analyses on the NGA database were used as a benchmark to investigate near-source effects in the recent April 6th 2009 L'Aquila earthquake. In particular horizontal strike-rotated records from the mainshock were analyzed. Extracted pulses and seismic demand of signals identified as pulse-like agree with the NGA results and seems to suggest that directivity effects occurred and that non-ordinary seismic demand affected near-source structures.

A few side results were also found. In fact, the fault parallel components of pulse-like stations were found to have an inelastic-to-elastic displacement ratio not

completely similar to that of ordinary records. Moreover, an analysis which includes the vertical components of motion did not provide clear evidence of directivity effects in the rupture-normal direction.

As a final conclusion, now that attempts to modify probabilistic seismic hazard analysis to account for near-source effects are close to succeed, these results show also that specific modification to inelastic demand in regions close to faults should be taken into account in structural design procedures.

ACKNOWLEDGEMENTS

REFERENCES

1. Somerville, P. G., Smith, N. F., Graves, R.W., Abrahamson, N. A. (1997) Modification of Empirical Strong Motion Attenuation Relations to Include the Amplitude and Duration Effect of Rupture Directivity, *Seism. Res. Lett.,* 68(1), 199-122.
2. Singh, P. J. (1985) Earthquake Ground Motions: Implications for Designing Structures and Reconciling Structural Damage, *Earthquake Spectra* 1(2), 239-270.
3. Reiter, L. (1990) *Earthquake Hazard Analysis, Issues and Insights*, Columbia University Press, NY.
4. Somerville, P. G. (2005) Engineering Characterization of Near-Fault Ground Motions, *Proceeding of 2005 NZSEE Conference*, Wairakei, NZ.
5. Bray, J. D., Rodriguez-Marek, A. (2004) Characterization of Forward-directivity Ground Motions in the Near-fault Region. *Soil Dyn. Earthquake Eng.*, 24(11), 815-828.
6. Tothong, P., Luco, N. (2007) Probabilistic seismic demand analysis using advanced ground motion intensity measures, *Earthquake Eng. Struct. Dyn.*, 36, 1837–1860.
7. Boatwright, J. (2007) The Persistence of Directivity in Small Earthquakes, *Bull. Seism. Soc. Am.*, 97(6), 1850-1861.
8. Baker, J. W. (2007) Quantitative Classification of Near-Fault Ground Motions Using Wavelet Analysis, *Bull. Seism. Soc. Am.*, 97(5), 1486-1501.
9. Iervolino, I., Cornell, C. A. (2008) Probability of Occurrence of Velocity Pulses in Near-Source Ground Motions, *Bull. Seism. Soc. Am.*, 98(5), 2262-2277.
10. Baker, J. W. (2008) Identification of Near-Fault Velocity and Prediction of Resulting Response Spectra, *Proceeding of Geotechnical Earthquake Engn. Struct. Dyn. IV*, Sacramento, CA. [Available at http://www.stanford.edu/~bakerjw/Documents/Baker%20(2008)%20Pulse%20ID,%20 GEESD%20for%20distribution.pdf, last accessed 2009 august the 2nd.]
11. Boore, D. M., Atkinson, G. M. (2008) Ground-Motion Prediction Equations for the Average Horizontal Component of PGA, PGV and 5%-Damped PSA at Spectral Period between 0.01s and 10.0 s, *Earthquake Spectra*, 24(1), 99-138.
12. Beyer, K., Bommer, J. J. (2006) Relationships between Median Values and between Aleatory Variabilities for Different Definitions of the Horizontal Component of Motion, *Bull. Seism. Soc. Am.*, 96(4A), 1512-1522.
13. Somerville, P. G. (2003) Magnitude Scaling of the Near Fault Rupture Directivity Pulse, *Physics of the Earth and Planetary Interiors*, 137, 201-212.
14. Tothong, P., Cornell, C. A., Baker, J. W. (2007) Explicit Directivity-Pulse Inclusion in Probabilistic Seismic Hazard Analysis, *Earthquake Spectra*, 23(4), 867-891.

15. Hancock, J., Bommer, J. J. (2006) A State-of-Knowledge Review of the Influence of Strong-Motion Duration on Structural Damage, *Earthquake Spectra*, 22(3), 827-845.

16. Tothong, P., Cornell C. A. (2006) *Probabilistic Seismic Demand Analysis Using Advanced Ground Motion Intensity Measures, Attenuation Relationships, and Near Fault Effect*, PEER Report 2006/11, Pacific Earthquake Engineering Reserch Center, Berkeley, CA.

17. Abrahamson, N. A., Somerville, P. G. (1996) Effects of the Hanging Wall and Footwall on Ground Motions Recorded During the Northridge Earthquake, *Bull. Seism. Soc. Am.*, 86(1b), S93-S99.

18. CEN, European Committee for Standardisation (2003) *Eurocode 8: design provisions for earthquake resistance of structures, Part 1.1: general rules, seismic actions and rules for buildings*, prEN 1998-1.

19. Ameri, G., Massa, M., Bindi, D., D'Alema, E., Gorini, A., Luzi, L., Marzorati, S., Pacor, F., Paolucci, R., Puglia, R., Smerzini, C. (2009), The 6 April 2009, Mw 6.3, L'Aquila (Central Italy) earthquake: strong-motion observations, *Seism. Res. Lett.* (in press).

20. Verderame, G. M., Iervolino, I., Ricci, P. (2009) *Report on the Damages on Buildings Followings the Seismic Event of 6th of April*. [Available at http://www.reluis.it/doc/pdf/Aquila/Rapporto_fotografico_V1.2.pdf]

21. Akkar, S., Bommer, J. J. (2006) Influence of long-period filter cut-off on elastic spectral displacements. *Earthquake Eng. Struct. Dyn.*, 35(9), 1145–1165.

22. Chioccarelli, E., De Luca, F., Iervolino, I. (2009) *Preliminary Study of L'Aquila Earthquake Ground Motion Records*. [Available at http://www.reluis.it/doc/pdf/Aquila/Peak_Parameters_L_Aquila_Mainshock_V5.2.pdf]

23. Cosenza, E., Manfredi, G., Ramasco, R. (1993) The Use of Damage Functionls in Earthquake Engineering: A Comparison between Different Methods. *Earthquake Eng. Struct. Dyn.*, 22(10), 855-868.

24. Paolucci, R. (2009) Long-Period Earthquake Ground Motion: Recent Advances and Observations from the April 6 2009, M_w 6.3 L'Aquila Earthquake, Italy, *Proceeding of Aces Workshop on Performance-Based Earthquake Engineering Corfù, Greece*.

25. Sabetta, F., Pugliese, A. (1996) Estimation of Response Spectra and Simulations of Nonstationary Earthquake ground Motion, *Bull. Seism. Soc. Am.*, 86(2), 337-352.